# 11370: HICO CALIBRATION ANALYSIS TWO YEARS POST LAUNCH

**Karen W. Patterson and Jeffrey H. Bowles**
Naval Research Laboratory, Remote Sensing Division, Code 7231, 4555 Overlook Ave SW, Washington, DC 20375
E-mail: karen.patterson@nrl.navy.mil

## ABSTRACT

Soon after the Hyperspectral Imager for the Coastal Ocean (HICO) started collecting imagery in September 2009, it became apparent that direct application of laboratory derived corrections and calibration coefficients resulted in at sensor radiances that were too low. Initial efforts to adjust the coefficients used in the calibration process resulted in HICO version 3 which is the first widely distributed data version. Since then, it has become clear that the initial adjustments are insufficient for some ocean color applications. Ocean color algorithms are very sensitive to even small errors in the calibrated at sensor radiances since water leaving radiance is often less than ten percent of the total at sensor radiance. Over the last couple of years, HICO has collected several thousand images including over one hundred diagnostic images such as dark scenes collected with the sensor in the stow position. This presentation summarizes efforts undertaken since the HICO version 3 release to refine the level 0 to level 1 processing to produce data as close to ocean color quality as possible.

## DARK SUBTRACTION

The first step in processing raw counts to calibrated radiances is to subtract the dark current offset (Lucke et al., 2011; Montes, 2010). Each HICO scene consists of a 200-scan pre-dark collected 5 minutes prior to the first image frame, the 2000-scan image and a 200-scan post-dark collected 5 minutes after the last image frame. The dark scans are collected with the instrument in the stowed position and the sensor is moved out along the slit to the angle required to image the intended target. The sensor is powered off between collects so the camera is warming up as it is collecting data and there are no temperature control mechanisms on the HICO package. This warm-up affects the magnitude of the dark correction. To account for the warm-up during collection, a time-dependent dark correction is applied to the raw HICO counts as follows (Lucke et al., 2011):

$DN_{corrected} = DN_{L0} - [A_{p2} + B_p*\ln(1+(n-203)/t_s)]$
$A_{p2} = (A_{p1} + A_{p3})/2 + 1.2$
$A_{p1,3} = S_{1,3} - 1.12472\ Bp$
$B_p = b + 0.9\ (S_{avg}-221)/(285-221)$
$S_{avg} = (S_1 + S_3)/2$
$S_{1,3}$ = line averaged dark count for pre- and post-dark
b = 11.4 (11.4 for cold and 12.3 for hot)
$t_s = 41$
n = line number in the HICO L0 file (200 pre-dark, 2000 image, 200 post-dark)
$DN_{L0}$ = raw count from the HICO L0 file
$DN_{corrected}$ = dark-corrected count
Subscripts of S and $A_p$: 1=pre-dark, 2=image, 3=post-dark

b is the temperature-dependent coefficient which controls the rate at which the dark current subtraction increases during data collection and was initially estimated from laboratory testing. The dark subtraction value increases rapidly at the beginning of the collect and levels off towards the middle and end of each segment. Between the launch of HICO in September 2009 and July 2011, 117 dark scenes were collected with the HICO sensor in the stow position for the pre-dark, scene and post-dark data segments. The darks scenes were analyzed to assess the validity and stability of this laboratory-derived dark correction.

As is standard in HICO processing, the first 3 scans of each segment were eliminated as it takes a few scans for the well charge to stabilize. During initial quick looks at the pre- and post-dark segments, individual spikes on the order of several hundred counts were discovered. To eliminate these anomalous data spikes, a despike filter was applied to the pre- and post-dark data prior to analysis. If an individual data value was outside 3 standard deviations of the prior and subsequent 5 data values collected for that band and pixel location in the array then the anomalous data value was replaced with the median of the prior and subsequent 5 data values. In prior HICO processing, anomalous values were simply deleted. However since the dark current increases during data collection, if multiple spikes were to be concentrated in one portion of the dark collection the dark average may be significantly altered, so replacement of the anomalous value with the median was chosen here. Spikes have been infrequent so the change to use the median is more a data quality insurance measure should the condition arise in the future. Pre-analysis preparations also included extracting the HICOCAMERATEMP value from the HREP health and status files for the first frame of each of the three image segments to assess the b coefficient stability as the package temperature varies during the light/dark cycles on orbit. The HICOCAMERATEMP value is an indicator of the package temperature and not the focal plane array temperature and ranged from 18.8-39.9°C. As such it only supports analyses based on scene averages. Scan line level detailed analysis of dark current versus temperature would not be supported and were not investigated.

Since the dark value increases rapidly as the sensor is first powered up and then levels off, pre- and post-dark averages were calculated using the entire segment (minus the first three scans) and just the last 100 scans of each dark segment. Then the averages were plotted versus the corresponding HICOCAMERATEMP for the 117 scenes analyzed (Figure 2). The dark values calculated using the last 100 scans were ~8 counts higher than the averages calculated using the entire dark segment. There was no significant change in variability of pre- and post-dark averages with temperature using 197 scans versus 100 scans. The scenes analyzed covered a wide temperature range so the existing method of using the entire pre- and post-dark segments minus the first three scans to calculate the dark averages is sufficient.

In the dark correction equation above, if the image segment is collected with the instrument in the stow position, then the entire dark-subtracted $DN_{corrected}$ image should consist of zero values. To see if the existing method is sufficient, the equation above was applied to the 117 dark scenes. Then 100-line averages were calculated for all sample positions across the array and all bands for the beginning (lines 10-109), middle (lines 950-1049) and end (lines 1900-1999) and plotted versus the HICOCAMERATEMP for the first image frame (Figure 3). Using the existing b value of 11.4 the 100-line averages at the beginning of the scene were OK, but the scene middle and end 100-line averages showed significant offsets, especially at the higher temperatures.

To assess the impact of temperature on the b coefficient, $DN_{corrected}$ was set to zero, the 197-scan pre- and post-dark averages were calculated and a new average b coefficient was determined for the image segment of each scene. The derived scene-average b values were plotted versus HICOCAMERATEMP for the first frame of the image segment (Figure 4). Variability in the b coefficient is evident and complex, though appears to be sufficiently characterized by piecewise linear relationships. To illustrate the impact of the b coefficient on the dark subtraction, HICO scene 1785 collected on February 1, 2010 and with a HICOCAMERATEMP of 34.63 was processed using the laboratory b value of 11.4 and the scene-derived b value of 13.21 (Figure 5). Since this is a dark scene, a quality dark correction will result in noise centered about zero in a plot of dark collected values versus image scan line. For scene 1785, dark corrected values are slightly negative at the beginning of the image and slightly positive for the majority of the rest of the image. When a b value of 13.21 is used, the dark corrected values properly center about zero for the entire image.

While results look promising when applying using a temperature-dependent b value in the HICO dark correction, some refinement may still be necessary. When a dark scene is collected, the sensor remains in the stow position and does not receive any external energy input. During normal imaging the sensor will be receiving reflected solar energy from the target scene. This additional energy may influence the overall magnitude and/or rate of change in the baseline/dark counts and has not been considered in this analysis.

## SMEAR AND SECOND ORDER

Smear correction is applied after dark (Lucke et al., 2011, Montes, 2010). The frame transfer time and exposure time for the smear correction are both being verified. Also, there is a known small, but non-negligible difference in the exposure time between the software/hardware configurations in diagnostic lab configuration and in flight configuration which must be verified. In addition, the HICO sensor has 170 bands of which only the first 128 bands are recorded. Assumptions must be made about the values contained in the unrecorded bands in order to apply the smear correction.

Following smear correction is second order light correction. The second order light correction in Lucke et al. (2011) was used in the initial HICO processing, but since has been replaced with an empirically-derived set of coefficients for wavelengths greater than 860nm. As dark and smear corrections are modified, adjustments to empirically-derived second order coefficients can be expected.

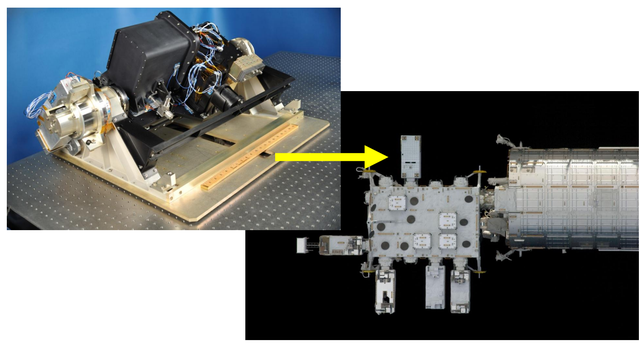

**Figure 1.** HICO and its position within HREP (HICO-RAIDS (Remote Atmospheric and Ionospheric Detection System) Experiment Payload) on the JEM-EF.

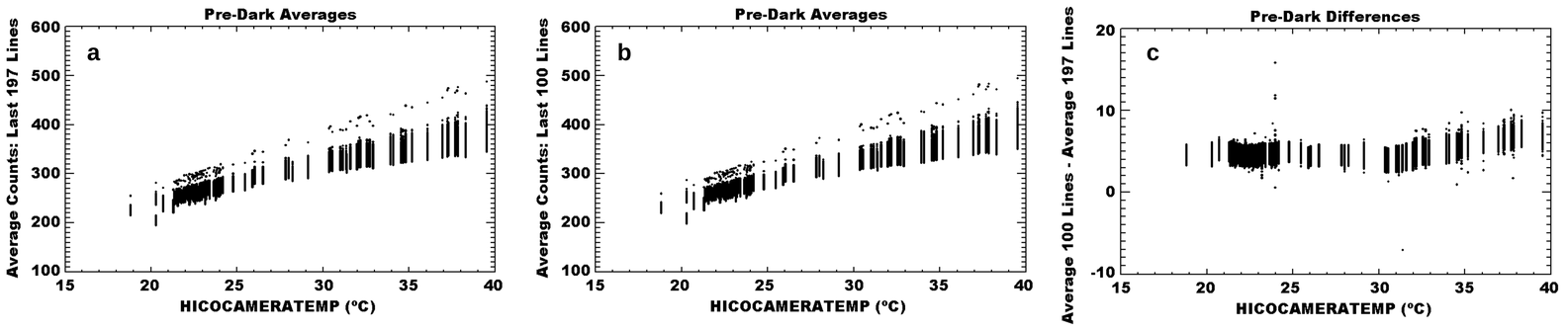


**Figure 2:** Pre-dark average counts for all 117 dark scenes and all 128 bands plotted as a function of camera temperature (a) for all except the first 3 lines and (b) for the last 100 lines. (c) is the difference between the 100-line and 197-line averages.

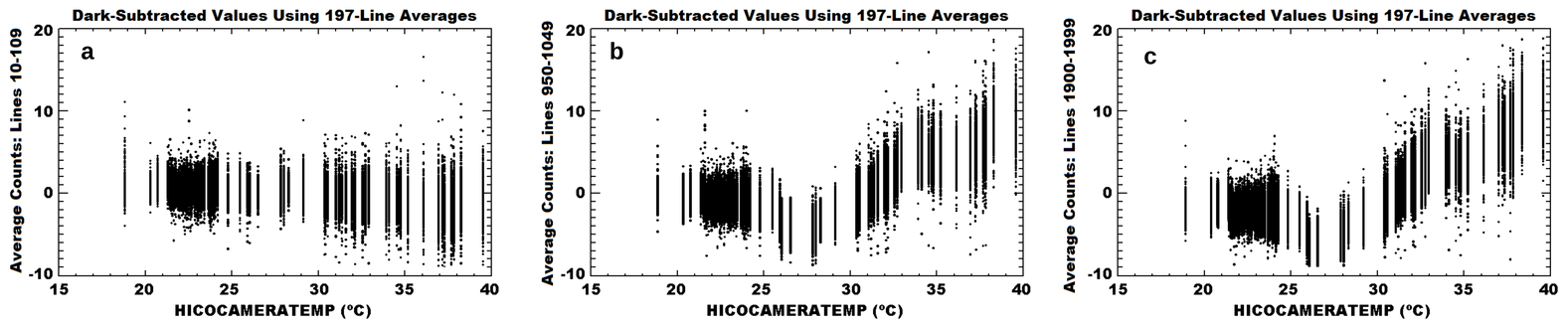


**Figure 3:** 100-line averages calculated for all 117 dark scenes and all 128 bands plotted as a function of camera temperature at the (a) beginning, (b) middle and (c) end of the scene. The b coefficient was set to 11.4 for these plots.

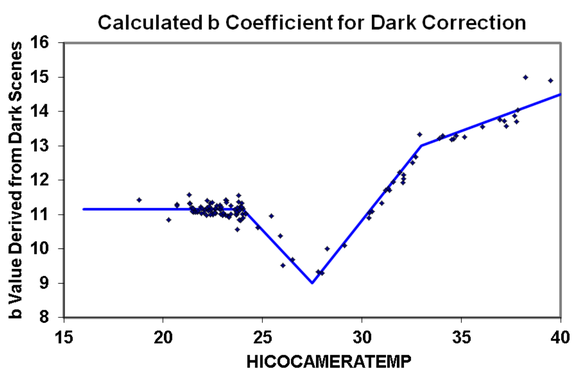


**Figure 4:** Full scene b coefficient averages calculated from inverting 117 dark scenes. All bands were combined in the average. Piecewise linear fits are shown in blue.

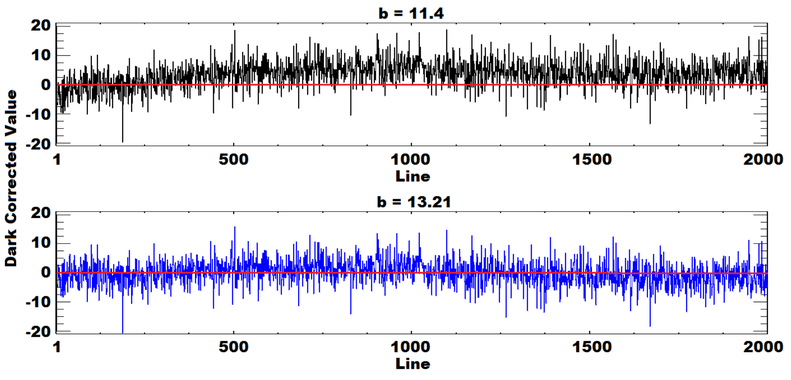


**Figure 5:** HICO scene 1785, band 20, sample 201corrected using a b value of 11.4 (upper) and 13.21 (lower). Noise is properly centered about zero for the entire scene when processed with a b value of 13.21.

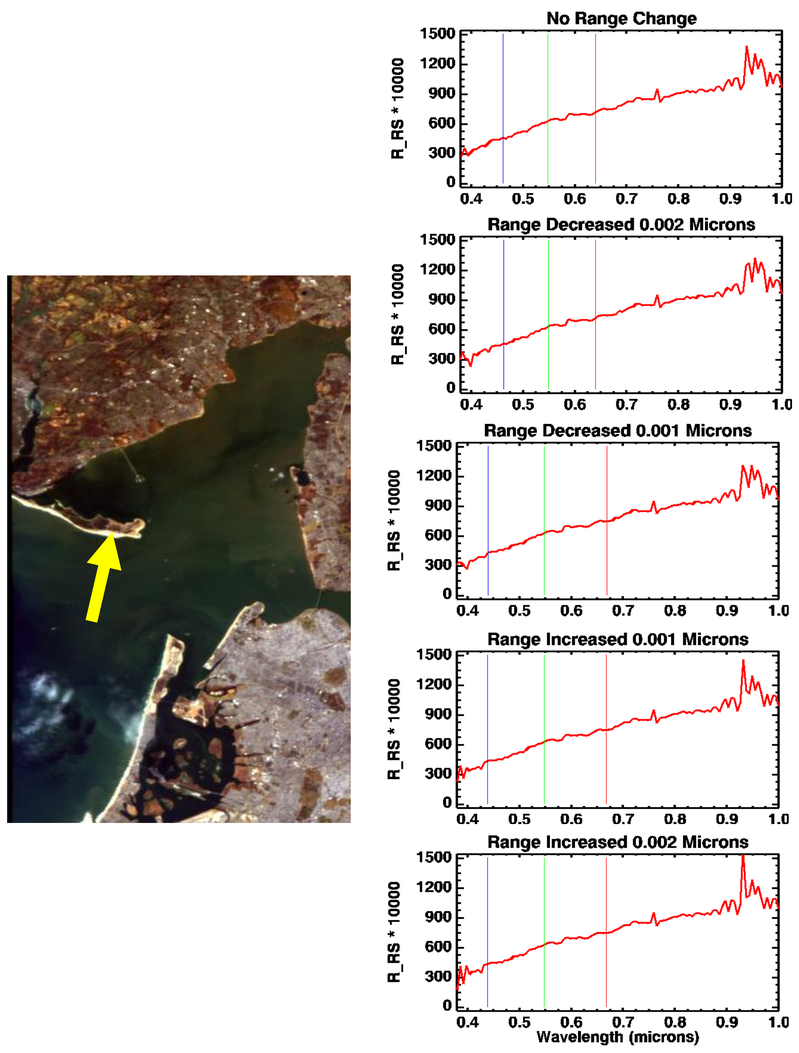


**Figure 6:** Example of spectral analysis for optimizing dispersion for a beach pixel (yellow arrow). A wavelength shift of -0.62 nm and FWHM of 5.5nm has already been applied. Total wavelength range was unchanged, compressed by 1-2 nm or expanded by 1-2 nm as indicated in the plot titles. Note spectral changes at shorter wavelengths

## ACKNOWLEDGMENTS

•Thanks to the Office of Naval Research for the funding without which this work would not have been possible.

## INTRODUCTION

During initial analysis of early post-launch HICO images a dark stripe was discovered along one side of the image indicating a slight alignment shift during launch. Most, if not all elements involved in the calculation of calibrated radiances from raw instrument counts may be affected by such a shift including the spectral wavelength calibration. Determining post-launch coefficients for each of the corrections involved in the raw count to radiance calculation is difficult as the instrument is no longer available for controlled laboratory testing and alterations made to one correction may cause problems to arise in subsequent corrections. In addition, several images are often required to empirically derive new coefficients which may be drifting as the sensor ages. The following is a summary of some of the calibration-related investigations performed in the two years since HICO was launched in September 2009 with emphasis on the dark correction.

## WAVELENGTH, DISPERSION, FWHM & SCALE FACTORS

Calibration scale factors and spectral wavelength calibration analysis are currently under evaluation. Analysis of distinct stable features such as the 760nm oxygen line are being used for wavelength calibration and based on such analyses it appears there was significant drift in the wavelength calibration during the early months post-launch. The wavelength shift and the alignment shift evidenced by the dark stripe on the side of the HICO images impact the calibration scale factors, Scale factor analysis will not be complete until these two effects are well characterized. Polarization effects are also being evaluated.

Wavelength, dispersion and full-width at half maximum (FWHM) were evaluated for an image collected of the Long Island Sound and surrounding areas of New York collected January 18, 2010. The HICO image was processed through the version 3 processing (Montes, 2010) with spectral smoothing turned off. Values for all three elements were adjusted and the images were atmospherically corrected using Tafkaa 6S (Montes et al., 2004) with local Aerosol Robotic Network (AERONET, http://aeronet.gsfc.nasa.gov) aerosol parameters from the LISCO site to remote sensing reflectances. Features such as the 760nm oxygen line were analyzed for several surface types. Optimal settings were determined as the values which produced minimal distortion at the edges of spectral features and minimized any spectral noise features in portions of the remote sensing reflectance spectra that should be smooth. A wavelength shift of -0.62nm, FWHM value of 5.5nm and no change to the original HICO lab-derived dispersion provided the optimal results for this image (Figure 6).

## SUMMARY

All coefficients and algorithms used in the processing of HICO data from raw counts to calibrated at sensor radiances continue to be evaluated. Many of the coefficients derived depend on other corrections applied during processing so optimization is an iterative process. The temperature range experienced by the sensor is much larger than anticipated and it has become clear that temperature-dependence needs to be evaluated as well. Evaluation of polarization effects on ocean scenes is also just beginning and is something to look for in the near future.

## REFERENCES

1. R. L. Lucke, M. R. Corson, N. R. McGlothlin, S. D. Butcher, D. L. Wood, D. R. Korwan, R.-R. Li, W. A. Snyder, C. O. Davis, and D. T. Chen, 2011. "The Hyperspectral Imager for the Coastal Ocean (HICO): Instrument Description and First Images: Applied Optics, v. 50(11), p. 1,501-1,516, doi:10.1364/AO.50.001501.
2. Montes, M., "HICOTM 1.6 processing description," (01 June 2010, unpublished)
3. Montes, M., Gao, B. and Davis, C., "NRL atmospheric correction algorithms for oceans: Tafkaa user's guide," Naval Research Laboratory Tech Memo NRL/MR/7230—04-8760 (2004).